

# Simulation of printed-on-fabric assemblies

David Jourdan

Université Côte d'Azur, Université de  
Lorraine, Inria  
France

Victor Romero

Université Grenoble Alpes, Inria,  
CNRS, Grenoble INP, LJK  
France

Etienne Vouga

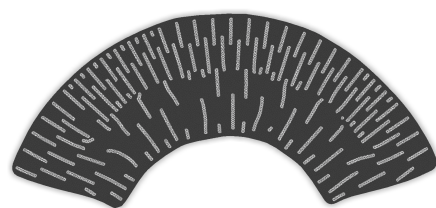
University of Texas at Austin  
USA

Adrien Bousseau

Université Côte d'Azur, Inria  
France

Mélina Skouras

Université Grenoble Alpes, Inria,  
CNRS, Grenoble INP, LJK  
France



(a) Input pattern



(b) Simulated shape



(c) Fabricated shape

**Figure 1:** *Printing-on-fabric* consists in depositing strips of plastic over a pre-stretched piece of fabric. On release, the forces exerted by the fabric make the overall structure buckle into a 3D shape. Our simulator predicts the 3D shape adopted by a given pattern of plastic strips by accounting for the physical properties of the fabric and its interactions with the plastic layer. Starting with this radial pattern to be printed on pre-stretched fabric (a), our simulator produces a toric shape (b) that closely matches the fabricated result (c).

## ABSTRACT

*Printing-on-fabric* is an affordable and practical method for creating self-actuated deployable surfaces: thin strips of plastic are deposited on top of a pre-stretched piece of fabric using a commodity 3D printer; the structure, once released, morphs to a programmed 3D shape. Several physics-aware modeling tools have recently been proposed to help designing such surfaces. However, existing simulators do not capture well all the deformations these structures can exhibit. In this work, we propose a new model for simulating printed-on-fabric composites based on a tailored bilayer formulation for modeling plastic-on-top-of-fabric strips, and an extended Saint-Venant–Kirchhoff material law for modeling the surrounding stretchy fabric. We show how to calibrate our model through a series of standard experiments. Finally, we demonstrate the improved accuracy of our simulator by conducting various tests.

## CCS CONCEPTS

• Computing methodologies → Physical simulation.

## KEYWORDS

additive manufacturing, self-shaping surfaces, textiles, printing-on-fabric

## ACM Reference Format:

David Jourdan, Victor Romero, Etienne Vouga, Adrien Bousseau, and Mélina Skouras. 2022. Simulation of printed-on-fabric assemblies. In *Symposium on Computational Fabrication (SCF '22)*, October 26–28, 2022, Seattle, WA, USA. ACM, New York, NY, USA, 11 pages. <https://doi.org/10.1145/3559400.3562001>

## 1 INTRODUCTION

Freeform surfaces appeal to designers and engineers for the combination of aesthetic and performance they can offer. But manufacturing, storing and transporting freeform surfaces is often more complex than dealing with flat pieces of material. This challenge has motivated research on *self-actuated structures* that can be manufactured flat before morphing to a curved state under the action of internal stress [Gu et al. 2019; Guseinov et al. 2017; Qamar et al. 2018]. Several research prototypes rely on expensive lab equipment and custom chemicals to program curvature into flat sheets of materials, such as liquid crystal elastomers [Aharoni et al. 2018], swelling gels [Kim et al. 2012], or elastomeric matrices [Boley et al. 2019]. In contrast, design enthusiasts have experimented with extruding patterns of molten plastic into pre-stretched fabric using commodity 3D printers [Erioli and Naldoni 2017]. This low-cost fabrication process, which we refer to as *printing-on-fabric*, allows the rapid prototyping of lightweight freeform structures that deploy into 3D when released (Figure 1).

Anticipating the 3D shape that a given structure will adopt under deployment is a difficult task, as that shape results from complex interplay between the elastic fabric and the flexible plastic. Practitioners thus need to engage in a tedious trial-and-error procedure to find patterns that yield interesting shapes once printed. Pérez et al. [2017] and Jourdan et al. [2020] proposed digital form-finding tools to assist in this task, but they focused on sparse networks of plastic strips for the former, and on a specific tiling of 3-pointed stars for the latter. We identified several shortcomings in both of these simulators, which prevent them from achieving predictive simulations for other types of patterns (Figure 12).

As noted by Jourdan et al. [2022], two physical phenomena contribute to the emergence of curvature in printing-on-fabric assemblies. First, the presence of incompressible plastic embedded into the fabric prevents the fabric to contract uniformly when plastic density varies over the surface. This non-uniform contraction results in a *frustration of metric*, which the structure accommodates for by buckling into 3D. However, because Pérez et al. [2017] and Jourdan et al. [2020] represent plastic strips with a reduced model that ignores their width, they over-estimate fabric contraction transversely to the strips. Second, by depositing melted plastic over pre-stretched fabric, the printing process results in a *bilayer structure* where the fabric layer exerts stress at its interface with the plastic layer, which the plastic also accommodates for by buckling into 3D. While Jourdan et al. [2020] accounted for this bilayer effect in their model, their solution was specific to thin rods and does not generalize to arbitrary patterns.

We propose several novel ingredients to accurately simulate printing-on-fabric assembly. In contrast to the rod-based models discussed above, we represent plastic strips with a surface-based representation that reproduces both the thickness as well as the spatial extent of the deposited plastic. Furthermore, we model this shell with a bilayer formulation [van Rees et al. 2017] that captures the interactions between the plastic strips and the underlying fabric. Finally, because the fabric is stretched well past its linear regime, we propose a non-linear fabric model that we calibrate via a series of real-world measurements. We evaluate the accuracy of our approach by simulating assemblies of increasing complexity, which we compare to real-world fabricated samples.

*Contributions.* In summary, we introduce:

- A tailored simulation method capable of accurately reproducing the 3D surfaces obtained when printing plastic strips over pre-stretched fabric.
- A custom fabric model that reproduces the non-linearity and anisotropy of real-world stretched fabric.
- A procedure to calibrate the fabric and plastic models using physical measurements.

## 2 RELATED WORK

*Printing-on-fabric.* The idea of creating curved surfaces by depositing a rigid material onto a pre-stretched substrate predates that of printing-on-fabric, as illustrated with early explorations by Oxman and Rosenberg [2007], who cast resin onto latex sheets. Designers Guberan and Clopath [2016] were among the first to deposit plastic onto pre-stretched fabric to create their Active Shoe. Since then, printing-on-fabric has attracted interest in architecture [Agkathidis

et al. 2019; Berdos et al. 2020; Kycia 2018, 2019], design [Erioli and Naldoni 2017; Fields 2018], and engineering [Schmelzeisen et al. 2018].

*Form-finding printed-on-fabric composites.* The first computer-aided method to design printed-on-fabric patterns [Pérez et al. 2017] focuses on sparse networks of connected curves, which gives rise to so-called *Kirchhoff-Plateau surfaces* that are only but a subset of the possible geometries that can be reached via printing-on-fabric. Because of their specific focus, Pérez et al. [2017] could afford approximations such as neglecting the bending resistance of the fabric or modeling the printed rods as 1D curves with infinitely small width, which do not hold for arbitrary patterns. Jourdan et al. [2020] propose a form-finding tool targeted at predicting the buckling behavior of arrangements of star-shaped plastic elements. They incorporated a bending term but they also neglect the fact that the printed plastic rods have a finite width. Both methods target specific pattern arrangements, and as such they miss important physical effects when applied to other designs.

Stapleton et al. [2019] use the FEM software Abaqus to simulate a simple rectangular shape printed on fabric and compared the printed results with the simulated one. By modeling explicitly the surface of the plastic as well as the fabric, their model seems better suited to accurately track local metric variations induced by the width of the printed rods. However, they model the fabric as an isotropic material, while our experiments suggest that stress in the fabric can double depending on the orientation of stretch (see Section 5).

*Bilayer shell simulation.* van Rees et al. [2017] propose a shell simulation method capable of modeling combinations of layers with different metrics by defining an *elastic energy inner product*. They show how to compute the first and second fundamental forms of the bilayer at rest as a function of the rest fundamental forms of the individual layers. Chen et al. [2018] use this method to simulate environmental effects such as moisture or temperature gradients. We adopt this framework to model the bilayer formed by the combination of plastic and fabric whose respective first fundamental forms and material properties can be combined into a reduced shell representation (see Section 4). Even though their method was based on a small-strain analysis, we show how to adapt it in our case where the fabric is stretched well past its linear regime.

*Fabric modeling.* Accurate reproduction of fabric's mechanical behavior has been an active research field. Our work fits in the category that models fabric as an homogeneous continuum and represents it as a thin shell. In particular, we draw inspiration from Volino et al. [2009] who proposed to account for the non-linearity of textiles' behavior through the use of custom non-linear stress-strain relations directly written in terms of the Green-Lagrange strain tensor. Following this type of approach, other data-driven, and often more sophisticated, material models were later presented. For example, Wang et al. [2011] introduce a piecewise linear material model and account for the bending resistance of the cloth. Miguel et al. [2012] use non-linear stress-strain laws with strain-dependent stiffness parameters represented by Hermite splines and fitted to data acquired using a custom stereo-based measurement system. In a subsequent work, they propose a stress-strain formulation based



on an isotropic Dahl’s model to reproduce the hysteresis observed in real fabric [Miguel et al. 2013]. Like us, Miguel et al. [2016] directly work on the energy density function to guarantee stress integrability, but their approach requires 3D data for calibration. By contrast, Clyde et al. [2017] rely on simpler standardized tests but their multi-stage optimization-based fitting procedure is rather involved. Closest to our work is that of Sperl et al. [2022] who also consider an augmented anisotropic Saint-Venant–Kirchhoff material law for their intermediate thin shell model. However, their model leaves aside path-dependent behavior such as hysteresis that is important for our targeted application.

Our goal is to model stretchy fabric (here, spandex) using an *energy-based* formulation that is *simple* (i.e. relies on a few coefficients that are easy to fit without resorting to complex optimization), *differentiable*, and that can be calibrated from *standard* tests. Moreover, we want our model to accurately reproduce the behavior of *prestretched* spandex *under release*, a deformation regime that has been mostly ignored. As far as we know, no previous model satisfies all these criteria at once.

### 3 OVERVIEW

In contrast to prior work that models plastic printed on fabric as infinitely-thin rods embedded into an elastic membrane [Jourdan et al. 2020; Pérez et al. 2017], we represent a printing-on-fabric assembly as an inhomogeneous thin shell composed of two different materials: a *fabric* material, and a *fabric-plastic bilayer* material. We discretize this shell as a triangular mesh, where each triangle is assigned one of the two materials (see inset). This approach allows us to account for the spatial extent of the plastic areas, which rod-based models ignore.

We model the fabric material with a custom formulation that accounts for the non-linearity and anisotropy we observed in real-world fabric, and model the bilayer material using the approach of van Rees et al. [2017]. We describe these two models in Section 4. We then detail how to calibrate our model from real-world measurements in Section 5.

## 4 MATERIAL MODELS

### 4.1 Modeling spandex

Spandex is a *heterogeneous* material made of a multitude of knitted synthetic fibers. The shape and alignment of the stitches (see inset figure) explain the high non-linearity and anisotropy of the material’s response to deformation. Besides, due to rearrangement of the fibers when the textile is stretched, this response is path-dependent. In our case, we are particularly interested in reproducing the behavior of the material when *unloaded*, i.e. released after being pre-stretched.

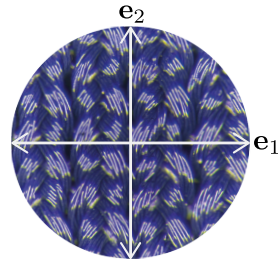
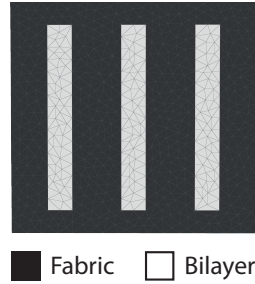


**Figure 2: Microscope view of the textile, with material axes overlaid.**

Rather than modeling spandex at the yarn level, which would result in accurate but costly simulations [Kaldor et al. 2008], we approximate its macro-scale behavior thanks to a – non-linear and orthotropic – custom *homogeneous* material model. As standard when modeling textiles [Miguel et al. 2012; Wang et al. 2011], we consider the in-plane and bending responses separately.

**Membrane model.** The Saint-Venant–Kirchhoff (StVK) material model is popular in Computer Graphics for modeling cloth, owing to its simplicity (see, e.g. [Volino et al. 2009]). However the linear relation between the second Piola–Kirchhoff stress tensor  $\mathbf{S}$  and the Green strain tensor  $\mathbf{E}$  it models does not capture well the hardening of knitted fabrics such as spandex when largely stretched (see stress-strain curves in Fig. 4, right). To address this limitation we propose to model spandex as an orthotropic StVK material augmented with two logarithmic terms such that the stress-strain relation, expressed in Voigt notation, takes the form

$$\mathbf{S} = \mathbf{C}\mathbf{E} - \sum_{i=1}^2 \beta_i \log\left(\frac{\gamma_i - E_{ii}}{\gamma_i}\right) \mathbf{e}_i, \quad (1)$$

where  $\mathbf{e}_i$ ,  $i = 1, 2$ , are the two axes of a Cartesian coordinate system aligned with the directions of the stitches (see Fig. 2),  $E_{ii}$  is the component of  $\mathbf{E}$  associated to the direction  $\mathbf{e}_i$ ,  $\beta_i$  and  $\gamma_i$ ,  $i = 1, 2$ , are material constants to be determined, and  $\mathbf{C}$  is a fourth-order tensor, the so-called elasticity tensor, represented here by a  $3 \times 3$  matrix, to be also fitted. Following Li and Barbič [2014], we assume the elasticity tensor  $\mathbf{C}$ , that encodes an orthotropic material, can be written as

$$\mathbf{C} = \frac{1}{1 - \nu_f^2} \begin{pmatrix} \alpha_1 & \sqrt{\alpha_1 \alpha_2} \nu_f & 0 \\ \sqrt{\alpha_1 \alpha_2} \nu_f & \alpha_2 & 0 \\ 0 & 0 & \alpha_3 (1 - \nu_f^2) \end{pmatrix} \quad (2)$$

with unknown stiffness parameters  $\alpha_1$ ,  $\alpha_2$  and  $\alpha_3$  and Poisson’s ratio  $\nu_f$ .

In the small strain regime, i.e. when the components of  $\mathbf{E}$  are small, Equation 1 reduces to a typical linear law. The vertical asymptote when  $E_{ii}$  tends to  $\gamma_i$  reproduces well the high increase of the material resistance when stretch becomes large. When there is no deformation, the division by  $\gamma_i$  in the log terms ensures that these terms do not bring any non-physical stress.

Since  $\mathbf{S}$  is defined as the partial derivative of the energy density of the material with respect to  $\mathbf{E}$ , we recover the corresponding energy density  $\Psi$  by integrating Equation 1 with respect to  $\mathbf{E}$ , which gives us

$$\Psi(\mathbf{E}) = \underbrace{\frac{1}{2} \mathbf{E}^T \mathbf{C} \mathbf{E}}_{\Psi_{\text{StVK}}} - \underbrace{\sum_{i=1}^2 \beta_i \left( (E_{ii} - \gamma_i) \log\left(\frac{\gamma_i - E_{ii}}{\gamma_i}\right) - E_{ii} \right)}_{\Psi_{\text{log}}}. \quad (3)$$

Note that  $\Psi$  is only defined for  $E_{ii} < \gamma_i$ . For practical purposes, we linearly extend the law beyond  $E_{ii} = \gamma_i - 10^{-6}$ .

It is well known that the StVK material model does not model high compression well and may lead to undesired inverted elements. By contrast, Neo-Hookean materials, thanks to their volume preserving term, do not suffer from this issue, as noted by Irving et al. [2004]. To avoid triangle collapse near the corners of the plastic strips, we blend our proposed material energy density  $\Psi$  with a

standard 2D isotropic Neo-Hookean energy of the form [Bonet and Wood 1997]

$$\Psi_{NH} = \frac{\mu}{2}(I_C - 2 - 2 \log J) + \frac{\lambda}{2}(\log J)^2, \quad (4)$$

where  $I_C = \lambda_1^2 + \lambda_2^2$  and  $J = \lambda_1 \lambda_2$ , with  $\lambda_1$  and  $\lambda_2$  the membrane principal stretches. The Lamé parameters  $\lambda$  and  $\mu$  are derived from the average Young's modulus  $E_f$  defined in Section 4.2 and the Poisson's ratio  $\nu_f$  using the relations  $\lambda = \frac{E_f \nu_f}{1 - \nu_f^2}$  and  $\mu = \frac{E_f}{2(1 + \nu_f)}$ . More specifically, using a small weighting factor  $\varepsilon = 0.01$ , we define our final spandex membrane energy as

$$\tilde{\Psi} = (1 - \varepsilon)\Psi + \varepsilon\Psi_{NH}. \quad (5)$$

In summary, our membrane energy density comprises three terms,  $\Psi_{SVK}$ ,  $\Psi_{log}$  and  $\Psi_{NH}$  and is parametrized by the eight parameters  $\alpha_1, \alpha_2, \alpha_3, \beta_1, \beta_2, \gamma_1, \gamma_2$  and  $\nu_f$  that we will fit to experimental data as described in Section 5.

In practice, we discretize our energies on a triangle mesh using linear elements (constant strain triangles) and we compute the total membrane energy by summing up individual triangle contributions as

$$W_{\text{membrane}} = h_f \sum_i \tilde{\Psi}(\mathbf{E}_i) \bar{A}_i, \quad (6)$$

where  $h$  is the fabric's height,  $\mathbf{E}_i$  is the Green strain tensor of triangle  $i$ , and  $\bar{A}_i$  the triangle's area at rest.

**Bending model.** We model the fabric's bending resistance using the discrete tangent-based bending energy by Tamstorf and Grinspun [2013] defined as

$$W_{\text{bending}} = k_B \sum_i \frac{3\|\bar{e}_i\|^2}{\bar{A}_i} \left( 2 \tan \left( \frac{\theta_i}{2} \right) \right)^2, \quad (7)$$

where  $\bar{e}_i$  is the rest length of edge  $i$ ,  $\bar{A}_i$  is the sum of the areas of the two incident triangles,  $\theta_i$  its dihedral angle and  $k_B$  is an average bending stiffness coefficient fitted according to the procedure described in Section 5.

## 4.2 Modeling plastic-on-fabric strips

We propose to model plastic-on-fabric strips as bilayers using the formulation of van Rees et al. [2017]. Considering the fabric and the plastic as two homogeneous monolayers glued to each other, with respective Young's moduli  $E_f$  and  $E_p$ , thicknesses  $h_f$  and  $h_p$ , and metrics  $\bar{\mathbf{a}}_f$  and  $\bar{\mathbf{a}}_p$ , the energy of the equivalent bilayer, parametrized on a 2D domain  $U$  with coordinates  $(x, y)$ , reads

$$\begin{aligned} W_{\text{bilayer}} = & \frac{1}{2} \int_U E_f \left[ \frac{h_f}{8} \|\bar{\mathbf{a}}_f^{-1} \mathbf{a} - \mathbf{I}\|^2 + \frac{h_f^3}{24} \|\bar{\mathbf{a}}_f^{-1} \mathbf{b}\|^2 \right. \\ & \left. + \frac{h_f^2}{8} \langle \bar{\mathbf{a}}_f^{-1} \mathbf{a} - \mathbf{I}, \bar{\mathbf{a}}_f^{-1} \mathbf{b} \rangle \right] \sqrt{\det \bar{\mathbf{a}}_f} \, dx \, dy \\ & + \frac{1}{2} \int_U E_p \left[ \frac{h_p}{8} \|\bar{\mathbf{a}}_p^{-1} \mathbf{a} - \mathbf{I}\|^2 + \frac{h_p^3}{24} \|\bar{\mathbf{a}}_p^{-1} \mathbf{b}\|^2 \right. \\ & \left. - \frac{h_p^2}{8} \langle \bar{\mathbf{a}}_p^{-1} \mathbf{a} - \mathbf{I}, \bar{\mathbf{a}}_p^{-1} \mathbf{b} \rangle \right] \sqrt{\det \bar{\mathbf{a}}_p} \, dx \, dy \end{aligned} \quad (8)$$

where  $\langle \mathbf{A}, \mathbf{B} \rangle = \frac{\nu_b}{1 - \nu_b} \text{tr}(\mathbf{A}) \text{tr}(\mathbf{B}) + \frac{1}{1 + \nu_b} \text{tr}(\mathbf{AB})$  is the elastic energy inner product associated to a material with Poisson's ratio

$\nu_b$  and Young's modulus pulled out,  $\|\mathbf{A}\|^2 = \langle \mathbf{A}, \mathbf{A} \rangle$  is the elastic energy norm,  $\mathbf{I}$  is the identity matrix, and  $\mathbf{a}$  and  $\mathbf{b}$  are, respectively, the first and second fundamental forms of the bilayer's midsurface in the current configuration.

In our setting, the fabric is uniformly stretched in all directions, so that  $\bar{\mathbf{a}}_f = \frac{1}{s^2} \mathbf{I}$ , with  $s$  denoting the stretching factor. The plastic has initially no residual strain, i.e.  $\bar{\mathbf{a}}_p = \mathbf{I}$ .

Note that the model above assumes isotropic linear material models for both the plastic strips and the fabric underneath. While modeling the non-linearity of the fabric behavior was important in areas with fabric alone, the linearity assumption of the fabric in the case of plastic-fabric assemblies is here reasonable as the in-plane deformation of the fabric, constrained by the plastic, remains limited. However, it is *essential* to account for the *pre-stretching* of the cloth. We also need to average the direction-dependent stiffnesses of the fabric to approximate it as an isotropic material and define a common Poisson's ratio  $\nu_b$ . Key to our model is therefore the choice of suitable parameters  $E_f$ ,  $E_p$  and  $\nu_b$ . Their estimation will be detailed in Section 5.

**Discretization.** We evaluate  $W_{\text{bilayer}}$  on a triangle mesh with elements conforming to the shape of the strips, and we assume that  $\mathbf{a}$  and  $\mathbf{b}$  are constant on each face. Following Chen et al. [2018], we approximate  $\mathbf{a}$  on the triangle formed by vertices  $\mathbf{v}_i, \mathbf{v}_j, \mathbf{v}_k$  as

$$\mathbf{a} = \begin{pmatrix} \|\mathbf{v}_j - \mathbf{v}_i\|^2 & (\mathbf{v}_j - \mathbf{v}_i) \cdot (\mathbf{v}_k - \mathbf{v}_i) \\ (\mathbf{v}_j - \mathbf{v}_i) \cdot (\mathbf{v}_k - \mathbf{v}_i) & \|\mathbf{v}_k - \mathbf{v}_i\|^2 \end{pmatrix},$$

and we compute  $\mathbf{b}$  using the "triangle with flaps" stencil of Grinspun et al. [2006] as

$$\mathbf{b} = \begin{pmatrix} (\mathbf{n}_j - \mathbf{n}_i) \cdot (\mathbf{v}_j - \mathbf{v}_i) & (\mathbf{n}_j - \mathbf{n}_i) \cdot (\mathbf{v}_k - \mathbf{v}_i) \\ (\mathbf{n}_k - \mathbf{n}_i) \cdot (\mathbf{v}_j - \mathbf{v}_i) & (\mathbf{n}_k - \mathbf{n}_i) \cdot (\mathbf{v}_k - \mathbf{v}_i) \end{pmatrix},$$

where  $\mathbf{n}_i, \mathbf{n}_j, \mathbf{n}_k$  are normals defined on the edges opposite to  $\mathbf{v}_i, \mathbf{v}_j, \mathbf{v}_k$  respectively, and computed by averaging the normals of their adjacent faces.

## 5 MEASUREMENTS AND FITTING

We now describe experiments we conducted to calibrate the simulation model presented above. We conducted these experiments on an elastic textile and a flexible plastic filament commonly used for 3D printing on stretched fabric. The textile is a finely-knitted spandex fabric composed of 80% polyamide and 20% elastane, while the printing filament material is TPU 95A (thermoplastic polyurethane with a 95A shore hardness).

The parameters of the membrane energy  $W_{\text{membrane}}$  depend on  $\alpha_1, \alpha_2, \alpha_3, \beta_1, \beta_2, \gamma_1, \gamma_2$  and  $\nu_f$ . We fit the stiffness coefficients  $\alpha_i, \beta_i$  and  $\gamma_i, i = 1, 2$ , using the stress-strain curves obtained from uniaxial tensile tests (see Section 5.1). We also use these tests to estimate the fabric's Poisson's ratio  $\nu_f$  using video data acquired during the tests. We obtain the shear modulus  $\alpha_3$  from the shear tests described in Section 5.2.

The bending energy  $W_{\text{bending}}$  of the textile depends on the bending stiffness coefficient  $k_B$ . We fit this parameter using the cantilever tests described in Section 5.3.

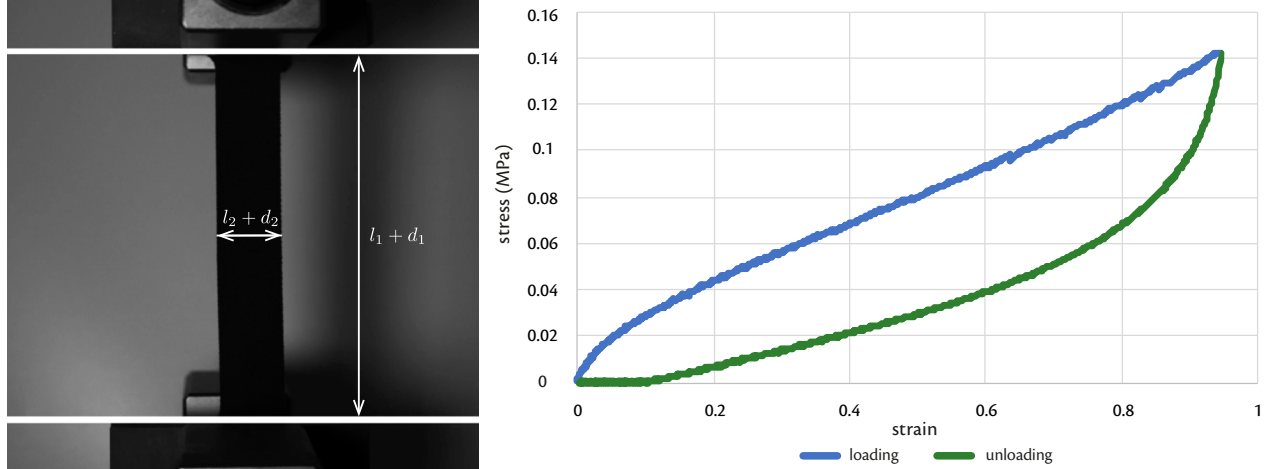


**Figure 3:** *left:* uniaxial stretch testing setup with initial lengths  $l_i$  and displacements  $d_i$  (note that the displacements  $d_i$  can be negative as is the case for  $d_2$ ), *right:* the stress-strain curve of a fabric sample forms a cycle because the followed path is not the same between loading and unloading.

### 5.1 Uniaxial stretch

The uniaxial tensile test consists in stretching a sample of material along a prescribed direction and recording the resulting stress as a function of the strain. We prepared material samples in a standard *dogbone* shape. The plastic was 3D printed into a 15 cm long by 1 cm wide shape with a similar printing orientation as the printed-on-fabric curves, while several fabric samples were laser cut out of a 11 cm long by 2 cm wide template. The fabric samples were cut out at different orientations to measure the orthotropy of the material. We measured the tensile response of samples oriented at, respectively, 0, 15, 30, 45, 60, 75, and 90° with respect to direction  $\mathbf{e}_1$  (see Fig. 2).

Fig. 3 (left) shows the rig setup we used to test our material samples. The tensile measurements were performed by an Instron 5865 machine with a 50 N force sensor which tracks both the displacement  $d_1$  of the clamped endpoints and the applied force  $f$  (called the *response* of the material). While performing these tests, we also record the material deformation *transverse* to the sample by filming the deformation and measuring the width of the sample at each frame. This data is used to compute the average Poisson's ratio of the spandex material.

The testing machine stretches and releases the samples by performing load-unload cycles, which creates loops characteristic of a hysteresis behavior when plotting the stress-strain curves, as shown in Fig. 3 (right). This path-dependent behavior is likely caused by internal friction between fibers of the fabric which rearrange as the textile gets stretched [Miguel et al. 2013]. Since we want to model the behavior of the textile once it has been stretched and gets released, we are interested in the *unloading* part of the curve (green in Fig. 3).

*Estimation of the Poisson's ratios  $\nu_f$  and  $\nu_b$ .* We start by estimating the fabric's average Poisson's ratio  $\nu_f$ , that will be needed to fit the other material parameters. Following Volino et al. [2009], we compute the strains  $E_{ii}$  with  $i = 1, 2$  (which correspond to the axial

and transverse directions respectively) the rest lengths  $l_i$  and the displacements  $d_i$  (see Fig. 3 (left)) as

$$E_{ii} = \frac{d_i}{l_i} + \frac{d_i^2}{2l_i^2}. \quad (9)$$

We approximate the Poisson's ratio for one orientation by averaging all the  $-\frac{E_{22}}{E_{11}}$  values over the course of the deformation. We then compute the final Poisson's ratio  $\nu_f$  to be used for the fabric's material model as the average over all sampled orientations. This value is estimated to be about 0.3.

Our bilayer model assumes the two monolayers it is composed of are made of homogeneous materials with same Poisson's ratio  $\nu_b$ . Since this is not the case here, we define  $\nu_b$  as the average of the Poisson's ratios of the two layers: for the fabric, we use the average Poisson's ratio  $\nu_f$  obtained above; for the plastic we use a value of 0.5 as the material used (thermoplastic polyurethane) is known to be almost incompressible [Qi and Boyce 2005]. Therefore,  $\nu_b$  is set to 0.4.

*Estimation of the fabric's membrane stiffness parameters  $\alpha_1, \alpha_2, \beta_1, \beta_2, \gamma_1$  and  $\gamma_2$ .* In Section 4, we defined the stress-strain relation of the spandex material in terms of the entries of the second Piola-Kirchhoff stress tensor  $\mathbf{S}$  and the non-linear Green strain tensor  $\mathbf{E}$ , better suited to model large deformations than the more conventional Cauchy stress and Cauchy strain tensors (see Equation 1). More specifically, letting  $S_{ii}$  and  $E_{ii}$  denote the normal components associated to the direction  $\mathbf{e}_i$  of, respectively, the stress tensor  $\mathbf{S}$  and the strain tensor  $\mathbf{E}$ , the relations between  $S_1, S_2, E_{11}$  and  $E_{22}$  read

$$S_{11} = \frac{1}{1 - \nu_f^2} \left( \alpha_1 E_{11} + \sqrt{\alpha_1 \alpha_2} \nu_f E_{22} \right) - \beta_1 \log \left( \frac{\gamma_1 - E_{11}}{\gamma_1} \right) \quad (10)$$

$$S_{22} = \frac{1}{1 - \nu_f^2} \left( \alpha_2 E_{22} + \sqrt{\alpha_1 \alpha_2} \nu_f E_{11} \right) - \beta_2 \log \left( \frac{\gamma_2 - E_{22}}{\gamma_2} \right). \quad (11)$$



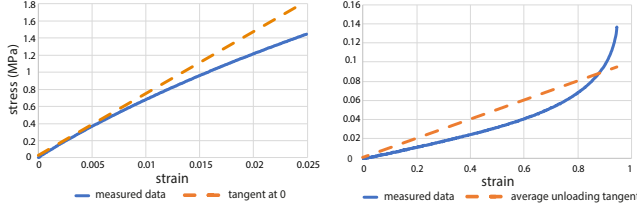


**Figure 4: left: stress-strain curve for the plastic material, the slope of its tangent at 0 is the material’s Young’s modulus; right: stress-strain curve for the fabric material, here we are interested in the slope of the tangent upon unloading.**

To fully decouple the stress-strain response along each material axis, and, in doing so, ease fitting of the stiffness parameters, we assume that the current transverse to axial strain ratio  $-\frac{E_{ii}}{E_{jj}}$ ,  $i \neq j$ , can be approximated by the average Poisson’s ratio  $\nu_f$ . This allows us to write the relation between  $S_{ii}$  and  $E_{ii}$  as

$$S_{ii} = \tilde{\alpha}_i E_{ii} - \beta_i \log\left(\frac{\gamma_i - E_{ii}}{\gamma_i}\right), \quad \text{with } \tilde{\alpha}_i = \alpha_i - \sqrt{\alpha_1 \alpha_2} \nu_f^2, \quad i = 1, 2. \quad (12)$$

After converting the measured force-displacement pairs on the  $0^\circ$  and  $90^\circ$  swatches into stress-strain data points using relations provided by Volino et al. [2009], we fit the  $\alpha_i$ ,  $\beta_i$  and  $\gamma_i$  parameters to the stress-strain data using non-linear least squares. Finally, we compute  $\alpha_1$  and  $\alpha_2$  from  $a_1$  and  $a_2$  by solving the  $2 \times 2$  system of equations.

Note that all these parameters depend on the stretching factor  $s$  of the fabric. In practice we fit them using fabric swatches stretched up to 45% and 70% of their initial lengths, and use linearly interpolated values when we need to model the fabric for different pre-stretching rates.

*Estimation of the fabric’s and plastic’s Young’s moduli  $E_f$  and  $E_p$ .* We use the stress-strain curves of the plastic and the different fabric samples to calibrate the bilayer material model (Equation 8), and in particular, to measure the Young’s moduli  $E_f$  and  $E_p$  of the two layers. To measure the Young’s modulus  $E_p$  of the plastic, we find the tangent at 0 of the stress-strain curve (Fig. 4, left), the slope of that tangent being the value of  $E_p$ . 3D printed objects are generally anisotropic and their response may vary depending on the orientation of the toolpaths used to fabricate them. We make sure that the toolpaths used for the measured sample are parallel to its main axis as it is the case for typical curves printed on fabric.

To estimate the Young’s modulus of the fabric substrate  $E_f$ , we follow a different procedure. Since the fabric material is pre-stretched to high strains when the plastic-fabric bilayer is formed, we are interested in its response for the full range of deformations, not just for strains close to zero. In fact, because the fabric is bounded by the plastic layer, it might never reach its original length. We account for such large deformations by computing the slope of a straight line approximating the full unloading part of the stress-strain curve (Fig. 4, right) for each sample orientation. The final value of  $E_f$  is thus computed as the average of all the slopes for each sample orientation.

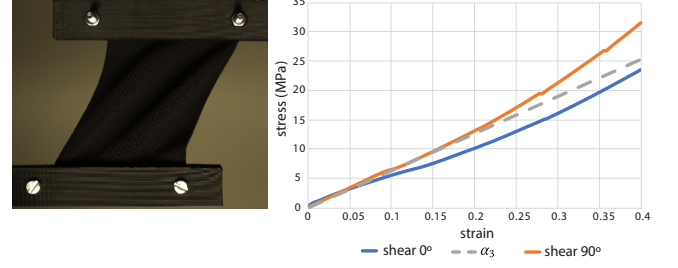


**Figure 5: left: shear testing setup right: stress-strain curves for a square sample oriented at  $0^\circ$  and  $90^\circ$ , and  $\alpha_3$  as a linear approximation of the average of both curves.**

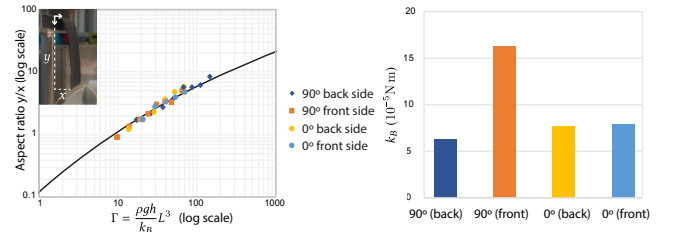


**Figure 6: Matching measurements of cantilevered shapes against the “master curve” of Romero et al. [2021].**

## 5.2 Shear tests

The last coefficient needed for the membrane parametric model is  $\alpha_3$  which corresponds to the shear modulus. To measure this coefficient we clamp two parallel edges of a square sample and move one of its edges laterally while probing the response (Fig. 5, left). We performed the measurement twice on the same sample according to two different orientations,  $90^\circ$  from each other. The results at  $0^\circ$  and  $90^\circ$  show an approximately linear response which corresponds well with the choice of expressing shear stress as a function of shear strain in our parametric stress-strain model (1). The two shearing experiments correspond to the same shear strain value and, as expected, lead to the same shear stress response in the linear regime, as evidenced by the common slope of the 2 curves at the origin. However, the behaviors of the  $0^\circ$  and  $90^\circ$  samples diverge for larger strain rates. We suspect this to be due, at least in part, to the anisotropy of the material. Our model cannot reproduce this orientation-dependent behavior and requires a single shear modulus  $\alpha_3$ , that we compute as the average linear regression of each curve.

## 5.3 Bending tests

The last coefficient needed for the fabric’s material model is the flexural coefficient  $k_B$  of the bending energy. This coefficient, for a homogeneous material with Young’s modulus  $E_f$ , thickness  $h_f$  and Poisson’s ratio  $\nu_f$ , is usually expressed as [Tamstorf and Grinspun 2013]

$$k_B = \frac{E_f h_f^3}{12(1 - \nu_f^2)},$$

but we can directly measure it by performing a cantilever test in which a fabric ribbon sample is clamped horizontally and a length  $L$  of itself is subjected to gravity. Romero et al. [2021] show the relationship between a unitless *gravito-bending* parameter  $\Gamma = \frac{\rho g h_f}{k_B} L^3$  – where  $\rho$  is the mass density and  $g$  is the acceleration of gravity – and the aspect ratio  $y/x$  of the bounding rectangle of the cantilevered sample (see Fig. 6, inset). This relationship is universal in the sense that the pair  $(\Gamma, y/x)$  will always be on a specific curve, called the *master curve*, no matter the material properties of the sample.

To find the value of  $k_B$ , we therefore measure  $y/x$  for different values of  $L$  and find the coefficient  $k_B$  such that the different points  $(\frac{\rho g h_f}{k_B} L^3, y/x)$  are as close as possible to the curve in the least squares sense. We performed the test on two different orientations of the fabric ( $0^\circ$  and  $90^\circ$ ) and tested them both front side up and back side up, for a total of 4 different experiments. The results (Fig. 6) show a difference in  $k_B$  between the  $0^\circ$  and  $90^\circ$  orientation, which is not surprising given the structure of the knitted textile. The difference between bending front side up and back side up was found to be negligible in the  $0^\circ$  case – meaning the resistance to bending is essentially symmetric in that direction – but for the  $90^\circ$  case the flexural coefficient is almost 3 times bigger on one side compared to the other, which can be explained by the fact that knitted textiles, in general, do not exhibit mirror symmetry between their front and back sides and therefore can have fairly different responses between bending upwards and downwards. The Discrete Shells model that we use to model bending does not account for these orientation and direction-dependent effects and is only weighted by one flexural coefficient  $k_B$ . Therefore, in practice, we compute  $k_B$  as the mean value between the 4 measured ones.

All the different parameters used in the bilayer model ( $E_f$ ,  $E_p$ ,  $\nu_b$ ), the membrane energy ( $\alpha_1$ ,  $\alpha_2$ ,  $\alpha_3$ ,  $\beta_1$ ,  $\beta_2$ ,  $\gamma_1$ ,  $\gamma_2$ ,  $\nu_f$ ) and the bending energy ( $k_B$ ) are summed up in table 1.

## 6 VALIDATION

We now describe several numerical experiments comparing the results of our simulator against real-world fabricated samples. We order the experiments by complexity, starting with empty fabric, then moving to the simulation of a single plastic strip, all the way to the simulation of doubly-curved surfaces.

*Fabric model.* Fig. 7 plots the forces integrated along each edge of a rectangular fabric sample undergoing uniaxial stretch, which reproduces the experiment shown in Fig. 3. Our simulator yields different forces depending on the orientation of the fabric sample, which matches the measurements well.

*Single plastic strip.* We first evaluate our simulator on a simple assembly composed of a single plastic strip printed on pre-stretched fabric, which curves to form a circular arc when released, as shown as inset.



We keep the length and width of the strip fixed and vary its thickness. As shown in Fig. 8, our simulator predicts that the curvature of the arc decreases as plastic thickness increases, and the curvature magnitude matches measurements on real samples. Note that the real-world measurements

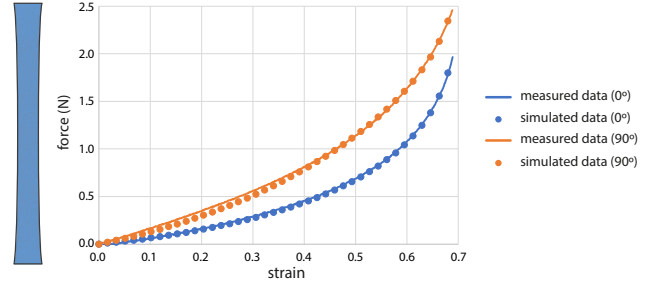


**Figure 7: Comparison between simulated force values and measurements for different orientations of a fabric sample undergoing uniaxial strain.**

exhibit variance, especially at low thickness due to printing imprecision.

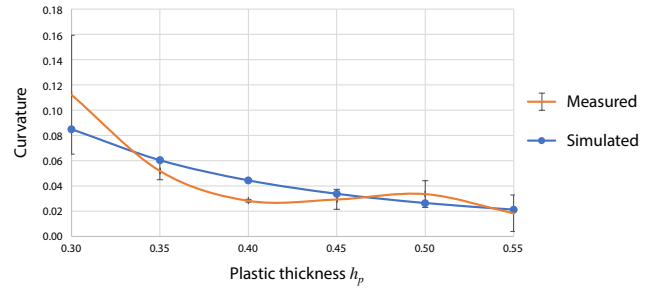


**Figure 8: Evolution of the curvature of a plastic strip printed on fabric as a function of plastic thickness. Error bars were computed over 5 measured samples.**

*Multiple parallel plastic strips.* We next evaluate the ability of our simulator to account for the interactions between fabric and plastic in the presence of multiple strips. We focus on the same pattern of staggered parallel strips as used by Jourdan et al. [2022], which yield cylindrical surfaces as the assembly rolls on itself when released (Fig. 9a,b). We keep the length and width of the strips fixed and vary their thickness  $h_p$  and spacing  $\mu$ . Fig. 10 plots the average curvature of the strips produced by our simulator against the curvature of real samples, which we measured by fitting a circle onto front-view pictures of the cylinders (Fig. 9c). We measured the curvature of samples printed on the front side as well as on the back side of the fabric, as we observed that fabric side impacts curvature, possibly because a different quantity of plastic is deposited depending on the roughness of the fabric surface (Fig. 11). Overall, our simulator reproduces well the curvature of real samples. First, curvature decreases as plastic thickness increases. Second, curvature increases as spacing between the strips increases, because more fabric exerts forces on each strip.

*Complex strip pattern.* Finally, we evaluate our simulator on a more complex assembly of radially-oriented strips with varying spacing, which should shape as a torus on release. Fig. 12 shows that our simulator effectively achieves a toric shape, while the simulator of Jourdan et al. [2020] under-estimates the curvature of the torus

$E_1$ (MPa)	$E_2$ (MPa)	$\nu_f$	$\alpha_1$	$\alpha_2$	$\alpha_3$	$\beta_1$	$\beta_2$	$\gamma_1$	$\gamma_2$	$k_B$ (N.m)
72.3	1.05	0.3	24161	90890	63419	29676	20512	0.9626	0.9637	$9.57 \times 10^{-6}$

Table 1: Parameters measured on a TPU95A filament and a spandex textile stretched up to 70% of its initial length.

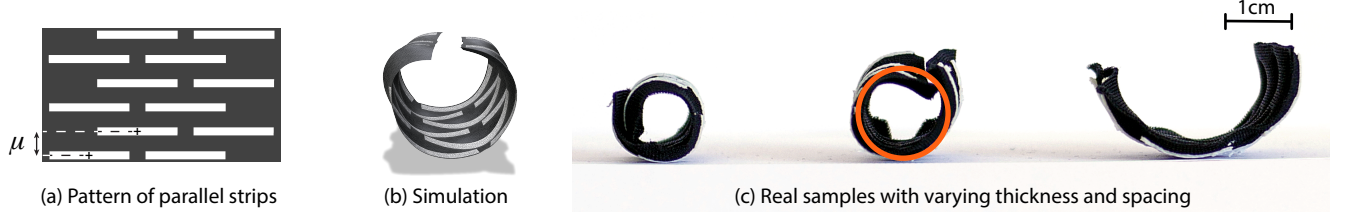


Figure 9: We focused our evaluation on a pattern of parallel plastic strips (a), which rolls as a cylinder when released. Our simulation reproduces well this behavior (b). We fabricated multiple such cylinders by varying the thickness  $h_p$  and spacing  $\mu$  of the strips (c), and measured their curvature by fitting a circle on their silhouette (c, orange circle).

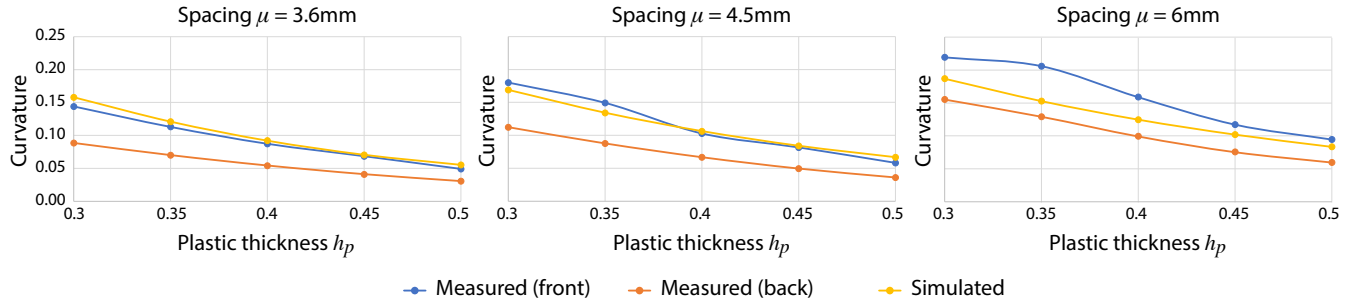


Figure 10: Evolution of the curvature of parallel plastic strips printed on fabric as a function of plastic thickness  $h_p$  and strip spacing  $\mu$ . Our simulator reproduces well the variations of curvature measured on real samples.

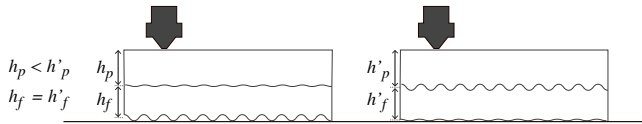


Figure 11: We hypothesize that fabric has a different roughness on each side. As a consequence, a different quantity of plastic is deposited, which would explain why we measured a different curvature depending on printing side (Fig. 10).

as it does not account for how the fabric contracts by a different amount transversely to the strips depending on strip density. While we used a procedural radial pattern for this experiment, Figure 1 demonstrates successful simulation of a pattern computed with the inverse-design method of Jourdan et al. [2022], achieving a good prediction of the shape obtained when printing the same pattern. Figure 13 provides additional visual comparisons between our simulations and fabricated assemblies obtained with patterns from Jourdan et al. [2022].

## 7 CONCLUSION

We have presented a physical model and calibration procedure dedicated to printing-on-fabric. By relying on a data-driven non-linear model for fabric, and on a bilayer shell for the plastic parts, our simulator better reproduces real-world fabricated artifacts than previous rod-based models. In particular, our model captures both the extrinsic curvature produced by plastic strips that bend as circular arcs, and the intrinsic curvature produced by the fabric that contracts non-uniformly depending on plastic density (Fig. 12).

We tested our model on patterns of locally-parallel strips, as proposed by Jourdan et al. [2022]. Yet, our model is generic and should also work for other patterns demonstrated in prior work, such as tilings of 3-pointed stars [Jourdan et al. 2020], curve networks [Pérez et al. 2017], or tilings of hexagons [Fields 2018]. An exciting direction for future work would be to integrate our simulator within an inverse-design algorithm, for instance to optimize the layout and thickness of plastic elements to best reproduce a target shape [Jourdan et al. 2022]. Indeed, accurate simulation has been critical for inverse design of other types of deployable structures, such as grid shells [Panetta et al. 2019] and inflatables [Panetta et al. 2021].



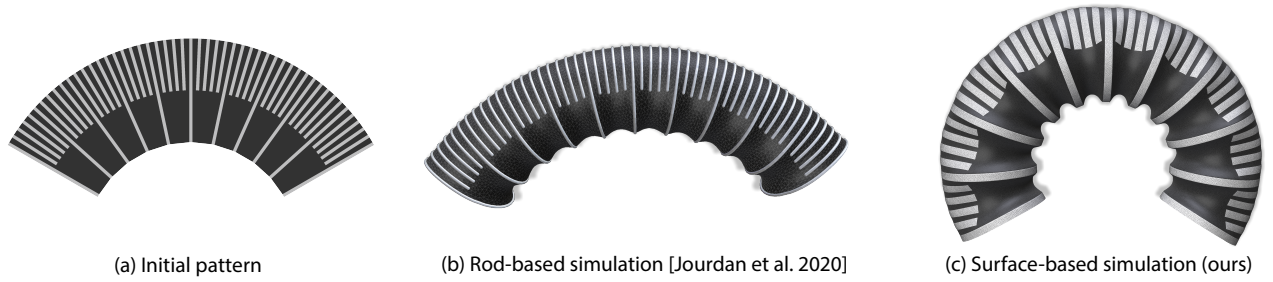


**Figure 12: Existing rod-based models fail to capture the intrinsic curvature induced by varying density of plastic strips over the surface. Starting with a procedural radial pattern of spatially-varying density (a), the simulator by Jourdan et al. [2020] contracts the pattern uniformly and only reproduces extrinsic curvature along the strips (b). In contrast, by modeling the plastic-fabric bilayer with a surface-based model, our approach captures well the non-uniform contraction transversely to the strip pattern, yielding the expected toric shape as the pattern contracts more along the inner boundary than along the outer one.**



**Figure 13: Visual comparison between the results of our simulator (b) and fabricated assemblies (c), using patterns computed with the inverse-design method of Jourdan et al. [2022] (a). The Skirt pattern (bottom row) contains strips printed on the back side of the fabric to produce negative extrinsic curvature.**

Our formulation and calibration protocol should also apply to other types of fabric, plastic, and amount of stretch. Our model

might also be extended to capture other phenomena, such as plasticity of the material. While Jourdan et al. [2020] accounted for

plasticity to reproduce the curvature of plastic rods, we did not find this effect necessary in our experiments. In addition, the bilayer model we rely on assumes isotropic plastic and fabric materials. It could be extended to account for the anisotropy of the fabric and further increase accuracy.

Finally, printing-on-fabric is a low-cost fabrication process that exhibits significant imprecision. In particular, it is common that the plastic extruded by the 3D printer does not adhere well to fabric due to under-extrusion, or leaks from one printed element to the next due to over-extrusion as the printing head moves over the surface. Such imprecision could be modeled explicitly by using a thermo-mechanical simulation of the plastic extrusion process, or implicitly by computing statistics about the frequency of various defects, and by propagating such uncertainty within the simulation of the fabric-plastic assembly.

## ACKNOWLEDGMENTS

This work was supported by the European Research Council (ERC) starting grants D<sup>3</sup> (ERC-2016-STG 714221), GEM (StG-2014-639139), by the US National Science Foundation (IIS-1910274), and research and software donations from Adobe Inc.

We thank the developers of the open source library Polyscope [Sharp et al. 2019] that we used for rendering the simulations. The fabricated models were photographed by Emilie Yu and were first published in [Jourdan et al. 2022].

## REFERENCES

- Asterios Agkathidis, Yorgos Berdos, and André Brown. 2019. Active membranes: 3D printing of elastic fibre patterns on pre-stretched textiles. *International Journal of Architectural Computing* 17, 1 (2019), 74–87. <https://doi.org/10.1177/1478077118800890>
- Hillel Aharoni, Yu Xia, Xinyue Zhang, Randall D. Kamien, and Shu Yang. 2018. Universal inverse design of surfaces with thin nematic elastomer sheets. *Proceedings of the National Academy of Sciences* 115, 28 (2018), 7206–7211. <https://doi.org/10.1073/pnas.1804702115>
- Yorgos Berdos, Asterios Agkathidis, and Andre Brown. 2020. Architectural hybrid material composites: computationally enabled techniques to control form generation. *Architectural Science Review* 63, 2 (2020), 154–164. <https://doi.org/10.1080/00038628.2019.1666357>
- J. William Boley, Wim M. van Rees, Charles Lissandrello, Mark N. Horenstein, Ryan L. Truby, Arda Kotikian, Jennifer A. Lewis, and L. Mahadevan. 2019. Shape-shifting structured lattices via multimaterial 4D printing. *Proceedings of the National Academy of Sciences* 116, 42 (2019), 20856–20862. <https://doi.org/10.1073/pnas.1908806116>
- Javier Bonet and Richard D. Wood. 1997. *Nonlinear continuum mechanics for finite element analysis*. Cambridge University Press, Cambridge. <https://doi.org/10.1017/CBO9780511755446>
- Hsiao-Yu Chen, Arnav Sastry, Wim M. van Rees, and Etienne Vouga. 2018. Physical Simulation of Environmentally Induced Thin Shell Deformation. *ACM Transactions on Graphics* 37, 4, Article 146 (July 2018), 13 pages. <https://doi.org/10.1145/3197517.3201395>
- David Clyde, Joseph Teran, and Rasmus Tamstorf. 2017. Modeling and Data-Driven Parameter Estimation for Woven Fabrics. In *Proceedings of the ACM SIGGRAPH/Eurographics Symposium on Computer Animation (SCA '17)*. Article 17, 11 pages. <https://doi.org/10.1145/3099564.3099577>
- Alessio Erioli and Lapo Naldoni. 2017. inFORMed Flexible matter workshop. <https://www.co-de-it.com/informed-flexible-matter.html>. Accessed: 2021-11-29.
- Gabe Fields. 2018. Self Forming Structures: An Exploration into 3D Printing on Pre-stretched Fabric. <https://n-e-r-v-o-u-s.com/blog/?p=8011> Nervous System.
- Eitan Grinspun, Yotam Gingold, Jason Reisman, and Denis Zorin. 2006. Computing discrete shape operators on general meshes. *Computer Graphics Forum* 25, 3 (2006), 547–556. <https://doi.org/10.1111/j.1467-8659.2006.00974.x>
- Jianzhe Gu, David E. Breen, Jenny Hu, Lifeng Zhu, Ye Tao, Tyson Van de Zande, Guanyun Wang, Yongjie Jessica Zhang, and Lining Yao. 2019. Geodesy: Self-Rising 2.5D Tiles by Printing along 2D Geodesic Closed Path. In *Proceedings of the 2019 CHI Conference on Human Factors in Computing Systems (CHI '19)*. Association for Computing Machinery, New York, USA, 1–10. <https://doi.org/10.1145/3290605.3300267>
- David Jourdan, Victor Romero, Etienne Vouga, Adrien Bousseau, and Mélina Skouras. 2016. Active Shoes. <http://www.christopheguberan.ch/active-shoes/>. Accessed: 2021-12-02.
- Ruslan Guseinov, Eder Miguel, and Bernd Bickel. 2017. CurveUps: Shaping Objects from Flat Plates with Tension-Actuated Curvature. *ACM Transactions on Graphics* 36, 4 (July 2017), 64:1–64:12. <https://doi.org/10.1145/3072959.3073709>
- G. Irving, J. Teran, and R. Fedkiw. 2004. Invertible Finite Elements for Robust Simulation of Large Deformation. In *Proceedings of the 2004 ACM SIGGRAPH/Eurographics Symposium on Computer Animation (SCA '04)*. Eurographics Association, Goslar, DEU, 131–140. <https://doi.org/10.1145/1028523.1028541>
- David Jourdan, Mélina Skouras, Etienne Vouga, and Adrien Bousseau. 2020. Printing-on-Fabric Meta-Material for Self-Shaping Architectural Models. In *Advances in Architectural Geometry 2020*. Presses des Ponts, Paris, FR, 264–285. <https://hal.archives-ouvertes.fr/hal-02925036>
- David Jourdan, Mélina Skouras, Etienne Vouga, and Adrien Bousseau. 2022. Computational Design of Self-Actuated Surfaces by Printing Plastic Ribbons on Stretched Fabric. *Computer Graphics Forum* 41, 2 (2022), 493–506. <https://doi.org/10.1111/cgf.14489>
- Jonathan M. Kaldor, Doug L. James, and Steve Marschner. 2008. Simulating Knitted Cloth at the Yarn Level. *ACM Transactions on Graphics* 27, 3, Article 65 (2008), 9 pages. <https://doi.org/10.1145/1399504.1360664>
- Jungwook Kim, James A. Hanna, Myunghwan Byun, Christian D. Santangelo, and Ryan C. Hayward. 2012. Designing Responsive Buckled Surfaces by Halftone Gel Lithography. *Science* 335, 6073 (2012), 1201–1205. <https://doi.org/10.1126/science.1215309>
- Agata Kycia. 2018. Material Form-Finding of Modular Textile Structures. In *CA<sup>2</sup>RE: Conference for Artistic and Architectural (Doctoral) Research*. Aarhus School of Architecture, Aarhus, DK, 331–341.
- Agata Kycia. 2019. Hybrid Textile Structures as Means of Material-informed Design Strategy. In *CA<sup>2</sup>RE Berlin Proceedings: Conference for Artistic and Architectural (Doctoral) Research*. Universitätsverlag der TU Berlin, Berlin, DE, 34–35.
- Yijing Li and Jernej Barbič. 2014. Stable Orthotropic Materials. In *Proceedings of the ACM SIGGRAPH/Eurographics Symposium on Computer Animation (SCA '14)*. Eurographics Association, Goslar, DEU, 41–46. <https://dl.acm.org/doi/10.5555/2849517.2849524>
- Eder Miguel, Derek Bradley, Bernhard Thomaszewski, Bernd Bickel, Wojciech Matusik, Miguel A. Otaduy, and Steve Marschner. 2012. Data-Driven Estimation of Cloth Simulation Models. *Computer Graphics Forum* 31, 2 (2012), 519–528. <https://doi.org/10.1111/j.1467-8659.2012.03031.x>
- Eder Miguel, David Miraut, and Miguel A. Otaduy. 2016. Modeling and Estimation of Energy-Based Hyperelastic Objects. *Computer Graphics Forum* 35, 2 (2016), 385–396. <https://doi.org/10.1111/cgf.12840>
- Eder Miguel, Rasmus Tamstorf, Derek Bradley, Sara C. Schwartzman, Bernhard Thomaszewski, Bernd Bickel, Wojciech Matusik, Steve Marschner, and Miguel A. Otaduy. 2013. Modeling and Estimation of Internal Friction in Cloth. *ACM Transactions on Graphics* 32, 6 (Nov. 2013). <https://doi.org/10.1145/2508363.2508389>
- Neri Oxman and Jesse Louis Rosenberg. 2007. Material-based Design Computation An Inquiry into Digital Simulation of Physical Material Properties as Design Generators. *International Journal of Architectural Computing* 5, 1 (2007), 25–44. <https://doi.org/10.1260/147807707780912985>
- Julian Panetta, Florin Isvoranu, Tian Chen, Emmanuel Siéfert, Benoît Roman, and Mark Pauly. 2021. Computational Inverse Design of Surface-Based Inflatables. *ACM Transactions on Graphics* 40, 4, Article 40 (July 2021), 14 pages. <https://doi.org/10.1145/3450626.3459789>
- J. Panetta, M. Konaković-Luković, F. Isvoranu, E. Bouleau, and M. Pauly. 2019. X-Shells: A New Class of Deployable Beam Structures. *ACM Transactions on Graphics* 38, 4 (July 2019), 83:1–83–15. <https://doi.org/10.1145/3306346.3323040>
- Jesús Pérez, Miguel A. Otaduy, and Bernhard Thomaszewski. 2017. Computational Design and Automated Fabrication of Kirchhoff-Plateau Surfaces. *ACM Transactions on Graphics* 36, 4 (July 2017), 62:1–62:12. <http://doi.acm.org/10.1145/3072959.3073695>
- Isabel P. S. Qamar, Rainer Groh, David Holman, and Anne Roudaut. 2018. HCI Meets Material Science: A Literature Review of Morphing Materials for the Design of Shape-Changing Interfaces. In *Proceedings of the 2018 CHI Conference on Human Factors in Computing Systems (Montreal QC, Canada) (CHI '18)*. Association for Computing Machinery, New York, USA, 23 pages. <https://doi.org/10.1145/3173574.3173948>
- Hang Jerry Qi and Mary C. Boyce. 2005. Stress-strain behavior of thermoplastic polyurethanes. *Mechanics of Materials* 37, 8 (2005), 817–839. <https://doi.org/10.1016/j.mechmat.2004.08.001>
- Victor Romero, Mickaël Ly, Abdullah Haroon Rasheed, Raphaël Charrondière, Arnaud Lazarus, Sébastien Neukirch, and Florence Bertails-Descoubes. 2021. Physical Validation of Simulators in Computer Graphics: A New Framework Dedicated to Slender Elastic Structures and Frictional Contact. *ACM Transaction on Graphics* 40, 4 (July 2021), 66:1–66:19. <https://doi.org/10.1145/3450626.3459931>
- David Schmelzeisen, Hannah Koch, Chris Pastore, and Thomas Gries. 2018. *4D Textiles: Hybrid Textile Structures that Can Change Structural Form with Time by 3D Printing*. Springer International Publishing, Cham, CH, 189–201. <https://doi.org/10.1007/978->

- 3-319-69050-6\_17
- Nicholas Sharp et al. 2019. Polyscope. [www.polyscope.run](http://www.polyscope.run).
- Georg Sperl, Rosa M. Sánchez-Banderas, Manwen Li, Chris Wojtan, and Miguel A. Otaduy. 2022. Estimation of Yarn-Level Simulation Models for Production Fabrics. *ACM Transactions on Graphics* 41, 4, Article 65 (July 2022), 15 pages. <https://doi.org/10.1145/3528223.3530167>
- Scott E. Stapleton, Dorit Kaufmann, Helga Krieger, Jan Schenk, Thomas Gries, and David Schmelzeisen. 2019. Finite element modeling to predict the steady-state structural behavior of 4D textiles. *Textile Research Journal* 89, 17 (2019), 3484–3498. <https://doi.org/10.1177/0040517518811948>
- Rasmus Tamstorf and Eitan Grinspun. 2013. Discrete Bending Forces and Their Jacobians. *Graphical Models* 75, 6 (Nov. 2013), 362–370. <https://doi.org/10.1016/j.gmod.2013.07.001>
- Wim M. van Rees, Etienne Vouga, and L. Mahadevan. 2017. Growth patterns for shape-shifting elastic bilayers. *Proceedings of the National Academy of Sciences* 114, 44 (2017), 11597–11602. <https://doi.org/10.1073/pnas.1709025114>
- Pascal Volino, Nadia Magnenat-Thalmann, and François Faure. 2009. A Simple Approach to Nonlinear Tensile Stiffness for Accurate Cloth Simulation. *ACM Transactions on Graphics* 28, 4, Article 105 (Sept. 2009), 16 pages. <https://doi.org/10.1145/1559755.1559762>
- Huamin Wang, James F. O'Brien, and Ravi Ramamoorthi. 2011. Data-Driven Elastic Models for Cloth: Modeling and Measurement. *ACM Transactions on Graphics* 30, 4 (July 2011), 71:1–71:12. <https://doi.org/10.1145/2010324.1964966>